

# Spatial methods for event reconstruction in CLEAN

Kevin J. Coakley <sup>a,\*</sup> and Daniel N. McKinsey <sup>b</sup>

<sup>a</sup>*Statistical Engineering Division, National Institute of Standards and Technology,  
325 Broadway, Boulder CO 80305*

<sup>b</sup>*Department of Physics, Yale University, New Haven, CT 06520*

---

## Abstract

In CLEAN (Cryogenic Low Energy Astrophysics with Noble gases), a proposed neutrino and dark matter detector, background discrimination is possible if one can determine the location of an ionizing radiation event with high accuracy. Here, we develop spatial methods for event reconstruction, and study their performance in computer simulation experiments. We simulate ionizing radiation events that produce multiple scintillation photons within a spherical detection volume filled with liquid neon. We estimate the radial location of a particular ionizing radiation event based on the observed count data corresponding to that event. The count data are collected by detectors mounted at the spherical boundary of the detection volume. We neglect absorption, but account for Rayleigh scattering. To account for wavelength-shifting of the scintillation light, we assume that photons are absorbed and re-emitted at the detectors. In our study, the detectors incompletely cover the surface area of the sphere. In the first method, we estimate the radial location of the event by maximizing the approximate Poisson likelihood of the observed count data. To correct for scattering and wavelength-shifting, we adjust this estimate using a polynomial calibration model. In the second method, we predict the radial location of the event as a polynomial function of the magnitude of the centroid of the observed count data. The polynomial calibration models are constructed from calibration (training) data. In general, the Maximum Likelihood method estimate is more accurate than that of the centroid method estimate. We estimate the expected number of photons emitted by the event by a Maximum Likelihood method and a simple method based on the ratio of the number of detected photons and a detection probability factor.

*Key words:* cryogenics, dark matter, event reconstruction, Monte Carlo, neutrinos, statistical methods

## 1 Introduction

We estimate the location of an ionizing radiation event that produces multiple photons within a spherical detection volume based on count data recorded by detectors mounted on the boundary of this detection volume. The detectors cover approximately 75 % of the total area of the detection volume boundary. We assume that all detected photons produced by a particular event can be distinguished according to their arrival times from photon counts produced by other events. Beyond this, we do not require additional temporal information. We assume that absorption is negligible, and that photons undergo Rayleigh scattering. We also estimate the expected number of emitted photons for the event.

Our “event reconstruction” work is motivated by a proposed experiment called Cryogenic Low Energy Astrophysics with Noble gases (CLEAN). In CLEAN [1,2], events would be detected based on scintillation light produced by neutrino-electron scattering and WIMP-nuclear elastic scattering in a large cryostat filled with liquid neon. In CLEAN, the expected number of scintillation photons produced by an event would be proportional to the amount of energy deposited by the event. The proportionality factor would be determined from a calibration experiment. Such events of interest would occur uniformly throughout the cryostat. Here, we consider a cryostat with a spherical geometry. Because neon has lower binding energy to surfaces than most radioactive impurities, there should not be internal backgrounds in the neon provided that the neon is purified using cold traps. Background gamma ray events would also produce scintillation light, and tend to occur near the walls. Near the center of a spherical detection volume, the penetration probability of background gamma rays is very low. Thus, if the radial position of an event can be determined accurately, background gamma ray events can be discriminated with high confidence from events of interest.

In this current paper, we focus solely on the event reconstruction problem. In a forthcoming paper, we will present a detailed simulation of CLEAN, including background gamma ray propagation. In this later paper, we will quantify the performance of our event reconstruction method for determining the location

---

\* Contributions of NIST staff to this work are not subject to copyright laws in the US.

*Email addresses:* kevin.coakley@nist.gov (Kevin J. Coakley), daniel.mckinsey@yale.edu (Daniel N. McKinsey).

of an event in the context of the physics goals of a CLEAN experiment. We will also discuss experimental design, calibration, and construction of CLEAN.

Temporal methods, not spatial methods, are commonly used for event reconstruction in the current neutrino experiments KamLAND [3,4] and Borexino [5]. Both of these experiments use organic scintillators. Here, we present a spatial method for event reconstruction and carefully study its performance in computer simulation experiments. We remark that the XMASS [6] research team is also studying spatial event reconstruction methods for their proposed neutrino experiment. Liquid xenon would be used as a scintillator in XMASS. In the field of tomography, spatial methods are commonly used to reconstruct spatially varying intensity images [7-11]. For each pixel or voxel, the corresponding intensity parameter is the expected number of photons emitted during the experiment. Instead of reconstructing a spatially varying photon intensity image, we seek to determine the intensity and location of a single source of photons. Thus, our problem is a special case of a more general imaging problem. In this work, we model the observed count data as a realization of a spatial Poisson process. This approach is frequently taken to solve a variety of imaging problems in nuclear medicine [8-11]. We estimate the event location by maximizing the approximate likelihood function of the observed detector count data assuming a scatter-free transition matrix. Because the transition matrix does not account for scattering, the estimate of the radial location of the event can be strongly biased. However, we significantly reduce this bias, that is, systematic error, by correcting the initial estimate based on a calibration model determined from calibration (training) data. This is possible because the bias of the estimate introduced by misspecification of the transition matrix has a very predictable structure.

We do not mean to imply that bias results only because of misspecification of the transition matrix. For the case where we use the exact transition matrix, we expect some bias because nonlinear estimation methods, including the Maximum Likelihood (ML) method, generally produce biased estimates. We expect this bias to be more significant for low count situations than for high count situations. For a general discussion of this point, see [12]. For a specific illustration of this point, see [13].

We stress that the methods we develop here are appropriate for the case where absorption of scintillation photons within the neon is negligible. For the case where absorption is significant, our methods are not directly applicable without further modification. If absorption effects are significant in the actual CLEAN experiment, we plan to directly estimate a transition matrix that will account for scattering, absorption, and other geometric effects. (This direct transition matrix modeling approach has been suggested in [6] for the planned XMASS experiment.) Even if we have exact knowledge of the true transition matrix, further calibration experiments may be necessary to quan-

tify the performance of CLEAN. The need for further calibration studies may be most pressing for low count situations.

In Section 2, we present the scattering model. In Section 3, we present a Poisson likelihood model for the data based on a scatter-free transition matrix. In Section 4, we study the statistical properties of both the uncorrected and corrected radial estimates for a variety of cases. For the same data, we compare a prediction model based on the centroid of the observed counts with the ML estimate. We also estimate the expected number of emitted photons at the event location using the ML method and a simpler method. In the simpler method, the estimate is proportional to the number of detected photons.

## 2 Simulation Model

At a particular location, multiple scintillation photons are produced by an event of interest. The probability density function (pdf) for the initial velocity direction of each emitted photon is uniform on the surface of the unit sphere. Following standard practice [14,15] we simulate the distance traveled before first scattering (as well as the distance between subsequent scatterings) by sampling from an exponential distribution. The expected value of this realization is the scattering length  $\lambda_s$ . At the point corresponding to the first scattering, we rotate the velocity direction about its original direction according to a model for the differential cross section of the Rayleigh scattering process. We neglect angular variation of the atomic form factor. Thus, the inner product of the new velocity direction and the old velocity direction,  $\cos(\theta)$ , has a pdf proportional to  $(1 + \cos^2(\theta))$ . We select a position on the cone defined by  $\cos(\theta)$  and the original velocity direction by sampling an azimuthal angle  $\phi$  that is uniformly distributed between 0 and  $2\pi$ .

We compute the point where a photon crosses the spherical boundary of the detection volume. If this point is not within the area of a detector, the photon is not detected. For the case where the crossing point is within the area covered by a detector element, we consider two detection models. In the “no-shift” model, the photon is detected by the detector element with probability  $p_e$ . We assume that  $p_e$  is independent of the photon trajectory with respect to the detector. In the “shift” model, the detector element absorbs the photon and converts it to lower energy. This wavelength-shifted photon is randomly re-emitted. We study the “wavelength-shifting” detection model because the extreme ultraviolet scintillation light that would be produced by liquid neon in CLEAN is not directly detectable by conventional detectors. However, after being shifted to a longer wavelength, this light is detectable by conventional detectors. The corresponding pdf of the velocity direction of the shifted photon is uniform on the surface of the unit sphere. If the shifted photon’s velocity

points radially outward, the re-emitted photon is detected with probability  $p_e$  at the detector element where shifting occurs. Otherwise, the photon travels inward, without scattering, until it crosses the spherical detection boundary. If this crossing point falls within the area covered by a detector element, it is detected with probability  $p_e$ . Otherwise, the photon is absorbed by the spherical wall and lost. Our assumption that the wavelength shifted photon does not scatter is based on the fact that the shifted photon has much longer wavelength (about 400 nm) than the original scintillation photon (about 80 nm), and Rayleigh scattering is much stronger at shorter wavelengths.

### 3 Estimation Method

#### 3.1 Likelihood Model

Given that a photon is emitted at location  $\mathbf{x}_s$ , the probability that the  $k$ th detector will detect this photon is denoted by  $P(k|\mathbf{x}_s, p_e)$  where  $p_e$  is the efficiency of the detector. By varying  $k$  and  $\mathbf{x}_s$ , we call the set  $P(k|\mathbf{x}_s, p_e)$  the probability transition matrix. For the “no-shift” detection model where there is no scattering, that is,  $\lambda_s = \infty$ , the transition matrix is

$$P(k|\mathbf{x}_s, p_e) = \frac{p_e}{4\pi} \int_{A_k} \frac{(\mathbf{x} - \mathbf{x}_s) \cdot \mathbf{x}}{|\mathbf{x} - \mathbf{x}_s|^3 |\mathbf{x}|} d\mathbf{x}, \quad (1)$$

where we integrate over the area of the  $k$ th detector. The expected number of detected photons at the  $k$ th detector is

$$\langle n_k \rangle = \lambda_k(\mathbf{x}_s) = \lambda P(k|\mathbf{x}_s, p_e), \quad (2)$$

where the intensity parameter  $\lambda$  is the expected number of photons emitted during the experiment. We approximate the integral in Eq. 1 as

$$P(k|\mathbf{x}_s, p_e) \approx \frac{p_e p_c R^2}{N_{det} |\mathbf{d}_k - \mathbf{x}_s|^2} \cos(\mathbf{d}_k - \mathbf{x}_s, \mathbf{d}_k), \quad (3)$$

where  $\mathbf{d}_k$  is the point where the  $k$ th detector is tangent to the sphere,  $p_c$  is the fractional area of the surface of the sphere covered by all detectors, and  $N_{det}$  is the number of detectors. We simulate data for  $N_{det} = 2072$  detectors tangent to the spherical boundary of the detection volume (Figure 1). We determine the tangent points by an optimal packing scheme [16].

The actual number of emitted photons at the event location is a realization of a Poisson process with intensity parameter  $\lambda$ . The expected value of the realization equals the intensity parameter. We assume that the number of counts at the  $k$ th detector is a realization of a Poisson process with intensity parameter  $\lambda_k$ . Thus, the Poisson log-likelihood function of the observed data is

$$\log L = \sum_k^{N_{det}} -\lambda_k(\mathbf{x}_s) + n_k \log(\lambda_k(\mathbf{x}_s)) - \log(n_k!), \quad (4)$$

where  $n_k$  is the number of detections at the  $k$ th detector. We estimate the model parameter vector  $\theta = (x, y, z, \lambda)$  by maximizing Eq. 4. Since, we use an inexact transition matrix, strictly speaking, we obtain an approximate ML estimate of the model parameters.

For the case where the transition matrix is exact, the  $(i, j)$ th component of the asymptotic covariance matrix of the ML model parameter is

$$\widehat{COV}(\hat{\theta}_i, \hat{\theta}_j) = (I^{-1})_{ij}, \quad (5)$$

where the Information matrix is

$$I_{ij} = \sum_{k=1}^{N_{det}} \frac{1}{\lambda_k} \frac{\partial \lambda_k(\mathbf{x}_s)}{\partial \theta_i} \frac{\partial \lambda_k(\mathbf{x}_s)}{\partial \theta_j}. \quad (6)$$

For the Poisson model,  $VAR(n_k) = \lambda_k(\mathbf{x}_s)$ . The asymptotic variance of the  $k$ th parameter estimate is the  $k$ th diagonal element of the asymptotic covariance matrix. The asymptotic standard error (s.e.) of the  $k$  parameter estimate is the square root of this asymptotic variance.

Our estimate of the radial location of the event is

$$\hat{r} = \sqrt{\hat{x}^2 + \hat{y}^2 + \hat{z}^2}. \quad (7)$$

For the special case where  $\mathbf{x}_s = (0, 0, z)$  and there is no scattering, we approximate the standard error of  $\hat{r}$  as

$$\sigma_{\hat{r}} \approx \sigma_{\hat{z}} = (I^{-1})_{33}. \quad (8)$$

For more details about asymptotic statistical theory, and a discussion of a closely related ML estimation problem involving Poisson data, see [17] and [13].

### 3.1.1 Efficient Simulation

If the detector efficiency  $p_e$  is much less than 1, many simulated photons are not detected even if they hit a detector element. Below, we describe an efficient simulation model which simulates the relevant fraction of emitted photons that are detected (provided that they hit a detector in the “no-shift” detection model or in the “shift-model” after wavelength shifting). On average, the relevant fraction that we simulate is  $p_e$ .

In our simulation model, we assume that the efficiency of the detector  $p_e$  is independent of the photon trajectory with respect to the detector. Thus,  $\lambda P(k|\mathbf{x}_s, p_e) = \lambda p_e P(k|\mathbf{x}_s, 1)$  (Eq. 2). Because of this relationship, we need not simulate trajectories for all simulated photons that are emitted at  $\mathbf{x}_s$ . In our efficient simulation model, the number of photons simulated is a realization of a Poisson process with expected value  $\lambda p_e$  rather than  $\lambda$ . However, in the efficient simulation model, the detector efficiency is 1 rather than  $p_e$ . That is, for data simulated with the efficient approach, we replace  $P(k|\mathbf{x}_s, p_e)$  with  $P(k|\mathbf{x}_s, 1)$ . In both simulation models, the simulated number of detected photons at the  $k$ th detector is a realization of a Poisson process with intensity parameter  $\lambda_k$ . Because of this substitution, we estimate a modified intensity  $\lambda p_e$  rather than the actual intensity  $\lambda$ . Throughout this work, we use this efficient approach.

### 3.1.2 Optimization Details

We seek the values of the model parameters that yield the global maximum (assuming that it is unique) of the approximate log-likelihood function,  $\log L$  (Eq. 4), using an iterative algorithm. Since optimization codes search for the global minimum of a cost function, we actually minimize  $-\log L$ . In each iteration, there are 3 steps.

1. Select initial values of parameter estimates.
2. Estimate model parameters by minimizing  $-\log L$  subject to the constraint that the event location is within the spherical detection volume.
3. Search for the global minimum of  $-\log L$  using the estimates from step 2 as initial values.

In step 1, for the first iteration, the initial estimate of the location of the event is the centroid of the observed count data. The initial estimate of the modified intensity parameter  $\lambda p_e$  is the number of observed counts divided by the coverage factor ( $p_c$ ). For subsequent iterations, the initial location is the sum of the centroid and a random perturbation vector. Each component is a normal (Gaussian) random variable with expected value equal to 0 and standard deviation equal to 0.05 R. We require that the location vector has

magnitude less than or equal to  $0.95 R$ . We perturb the initial estimate of  $\lambda p_e$  by multiplying  $n/p_e$  by a factor  $1 + \epsilon$ , where  $\epsilon$  is a normal random variable with expected value 0 and standard deviation 0.02.

In step 2, we minimize the sum of  $-\log L$  and a penalty function, using an algorithm based on a quasi-Newton method [18]. The penalty function forces the estimate to fall within the detection volume. The penalty function is 0 when  $\hat{r} < R$ , and  $10\,000 (\hat{r}/R)^2$  when  $\hat{r} \geq R$ .

In step 3, we minimize the cost function,  $-\log L$ , using a modified Newton method where we supply both the first and second derivatives of the cost function with respect to the model parameters [19].

In general, the numerical stability of the estimate depends on the number of counts, the scattering length, and the geometry of the detectors. For low count situations, stability is usually achieved by 30 iterations. For instance, for the case of wavelength-shifting and  $\lambda_s/R = 0.1$ , we simulate 500 events of interest for each of three cases. In the three cases, the number of observed counts  $n$  is 10, 25 and 50. For  $n = 10$ , the difference between the uncorrected estimate of  $\hat{r}/R$  at 30 and 90 iterations was greater than 0.01 only three times. For  $n = 25$  and  $n = 50$ , the difference between the estimate at 30 and 90 iterations was less than 0.01 for all 500 realizations. The number of cases for which the difference between the estimate at the first and 90th iterations was greater than 0.01 is respectively 14, 1, and 4 for  $n = 10$ ,  $n = 25$ , and  $n = 50$ . For all cases where the estimate at the first and 90th iterations varied by more than 0.01, the ‘‘instability’’ occurs at  $\hat{r}/R > 0.65$ . Hence, the outcome of a classification rule to determine if an event is either ‘‘background’’ or an ‘‘event of interest’’ is less sensitive to the number of iterations than is the point estimate of radial location. For all cases studied here, stable estimates are obtained by 30 iterations, provided that the number of detected photons is greater than 50.

### 3.2 Calibration Model

Our calibration model is

$$\frac{\hat{r}_c}{R} = \alpha_1 \frac{\hat{r}}{R} + \alpha_2 \left(\frac{\hat{r}}{R}\right)^2 + \alpha_3 \left(\frac{\hat{r}}{R}\right)^3, \quad (9)$$

where  $\hat{r}_c$  is the corrected estimate. We estimate the calibration model parameters,  $\alpha_1, \alpha_2, \alpha_3$ , from calibration data by minimizing



$$\sum_i (r_i - \alpha_1 \frac{\hat{r}_i}{R} + \alpha_2 (\frac{\hat{r}_i}{R})^2 + \alpha_3 (\frac{\hat{r}_i}{R})^3)^2, \quad (10)$$

where  $r_i$  and  $\hat{r}_i$  are the true and estimated values at the  $i$ th point in the calibration data set. The radial locations of the points in the calibration data are uniformly distributed (Table 1). We quantify the accuracy of the calibration model by computing  $\text{RMSE} = \sqrt{\frac{m}{m-k} \sum_{i=1}^m (\frac{\hat{r}_i}{R} - \frac{r_i}{R})^2}$ , where  $m$  is the total number of points in the calibration data set and  $k$  is the number of calibration model parameters. For the cases studied,  $m \approx 2500$ . In Table 1 and elsewhere, we represent the standard error, that is, the estimated standard deviation, of an estimate in parentheses. For instance, 0.894(16) means the estimated value is 0.894, and the associated standard error is 0.016.

In this work, we focus on estimation of the radial location of an event. If one wishes to estimate the Cartesian coordinates of the event, we suggest that the estimates of  $x, y$  and  $z$  are corrected in the same way as  $\hat{r}$ . That is,  $\hat{x}_c = \frac{\hat{r}_c}{\hat{r}} \hat{x}$ ,  $\hat{y}_c = \frac{\hat{r}_c}{\hat{r}} \hat{y}$ , and  $\hat{z}_c = \frac{\hat{r}_c}{\hat{r}} \hat{z}$ . In Figure 2, we illustrate how this approach works for an example.

## 4 Simulation Results

### 4.1 Position Estimation

In our first study, we simulate data at selected points on the  $z$ -axis of our detector coordinate system for the “no-shift” detection model. For each point, we simulate 100 data sets. The modified intensity parameter is  $\lambda p_e = 200$ . For the “no-shift” case, the bias of the uncorrected estimate increases as the scattering length decreases (Figure 3). This bias is expected because, in general, scattering increases the probability that a photon emitted in the upper hemisphere  $z > 0$  will cross the spherical boundary in the upper hemisphere. For instance, for the case where photons are emitted at  $\mathbf{x} = (0, 0, 0.9R)$ , the probability that the crossing occurs at  $z > 0.9R$  is 0.541(5), 0.708(5), 0.801(4) for  $\lambda_s/R = 1, 0.1, 0.01$ . This phenomenon appears to be related to the behavior of particles undergoing Brownian motion near absorbing walls [20].

The bias of the corrected estimate is significantly lower than the bias of the uncorrected estimate. In general, the RMSE of the corrected estimate decreases as the scattering length decreases. Moreover, the standard error of the corrected estimate is often below the asymptotic standard error computed from asymptotic theory for the scatter-free case. This is not inconsistent with statistical theory. Moreover, our estimation method exploits additional information provided in the calibration data that is not accounted for in the asymptotic

theory calculation. We stress that our results correspond to the case where absorption is negligible. For the more general case where absorption effects are significant, the accuracy of a corresponding prediction model may decrease as the scattering length decreases.

For the case where there is no scattering, that is,  $\lambda_s = \infty$ , “shifting” introduces a negative bias (Figure 4). For the “shift” model, as the scattering length decreases, the bias increases in general.

In CLEAN, events of interest would occur uniformly throughout the detection volume. Hence, the pdf for the radial location of an event of interest is proportional to  $r^2$ . We simulate events of interest that produce a fixed number of counts  $n$ . In Figure 5 we display scatterplots of the true value of  $r$  and the uncorrected estimated value of  $r$  for three cases. In CASE A, we consider the “shift” detection model where  $\lambda_s/R = \infty$ . In CASE B, we consider the “no-shift” detection model where  $\lambda_s/R = 0.1$ . In CASE C, we consider the “shift” detection model where  $\lambda_s/R = 0.1$ . In Figure 6, we display scatterplots of the true value of  $r$  and the corrected estimated value of  $r$  for the same three cases. In each scatterplot, we show the 0.1 quantile of the empirical distribution of the estimate as a dashed line and the level  $r_p/R = p^{1/3}$  where  $p = 0.1$  as a solid line. If our estimate  $\hat{r}$  were uniformly distributed in the spherical detection region, the fraction of estimates less than  $r_p = Rp^{1/3}$  would be  $p$ . Thus, ideally, for each value of  $n$ , one tenth of the estimates should fall below  $r_{0.1}$ .

Assuming that events that produce a fixed number of observed photons occur uniformly throughout the detection volume, the expected value of the fraction of corrected estimates of  $r$  below  $r_p$  divided by  $p$  is the efficiency of the detector. Ideally, the detector efficiency should be 1 for all  $n$ . However, our calibration model (Eq. 9) does not guarantee a detector efficiency equal to 1. Since a nonuniform detector efficiency as a function of  $n$  will distort the count spectrum of the detected events, one should quantify the detector efficiency. As an illustration, we estimate detector efficiency for the “shift” detection model where  $\lambda_s/R = 2/9$  (Figure 7).

For experiments like CLEAN, we wish to determine whether an event occurs within a particular inner spherical region or fiducial volume defined by  $r < Rp^{1/3}$ , where  $0 < p < 1$ . In principle, given enough calibration data, we can determine the radial boundary of a  $100 \times p$  percent fiducial volume so that the detector efficiency is arbitrarily close to 1 by setting  $r_p$  equal to the  $p$ th quantile of the distribution of estimated values of  $r$ . This classification problem can be viewed as a statistical hypothesis test where the null hypothesis is that the actual radial location of a particular event is a realization from a distribution that has a pdf proportional to  $r^2$ . In this way of looking at the problem, the estimated value of  $r$  (corrected or uncorrected) can be interpreted as the test statistic. We accept the null hypothesis if the test statistic falls below a

certain critical level. The  $p$ th quantile of the distribution of this test statistic (simulated under the assumption that the null hypothesis is true) is the critical level for a test with size  $1 - p$  [21]. For a test with size  $1 - p$ , when the null hypothesis is true, we reject it with probability  $1 - p$ . When one sets the critical level of a test with size  $1 - p$  to the  $p$ th quantile of a test statistic, one has calibrated a confidence point [22 page 263]. We wish to reject the null hypothesis with high probability when an event is due to background. That is, we wish the power of the test to be high. When events are due to background, a high rejection rate will yield a low background.

#### 4.1.1 Centroid Method

For comparison, we predict the radial location of an event based on the magnitude of the centroid of the count data. The centroid  $\vec{C}$  is defined to be

$$\vec{C} = \sum_k w_k \mathbf{d}_k, \quad (11)$$

where

$$w_k = \frac{n_k}{\sum_{j=1}^{N_{det}} n_j} \quad (12)$$

and  $n_k$  is the number of counts at the  $k$ th detector. Our Centroid method estimate of the radial location of the event is

$$\frac{\hat{r}_{centroid}}{R} = \beta_1 \frac{|\vec{C}|}{R} + \beta_2 \left(\frac{|\vec{C}|}{R}\right)^2. \quad (13)$$

In general, the variability of the Centroid method estimate (Figure 8, Table 2) is higher than that of the ML method (Figure 6, Table 1). The difference in performance is most dramatic for low count ( $n < 50$ ) cases.

## 4.2 Intensity Estimation

In the efficient simulation model, we simulate a Poisson random variable  $N$  with expected value equal to modified intensity  $\lambda p_e$ . To derive a simple estimate of the modified intensity, we assume that the number of detected counts  $n$ , given  $N$ , is a binomial random variable with expected value  $Np$  and variance  $Np(1 - p)$ . For the “no-shift” detection model  $p = p_c$ . For the “shift” detection model,  $p = p_c(1 - 0.5(1 - p_c))$ . Thus, our “naive” estimate of the modified intensity is

$$\widehat{\lambda p_e}_{naive} = \frac{n}{p}. \quad (14)$$

Our second estimate of the modified intensity is

$$\widehat{\lambda p_e}_{ML} = \frac{p_c \hat{\theta}_4}{p}, \quad (15)$$

where  $\hat{\theta}_4$  is the ML method estimate of  $\lambda p_e$  determined by maximizing the log-likelihood of the observed data (Eq. 4). We adjust  $\hat{\theta}_4$  because our transition matrix does not account for the effects of wavelength-shifting by the detectors. For the cases studied, for  $r/R < 0.9$ , the two methods yield similar results. However, for  $r \approx R$ , the variability of ML method estimate is generally higher than that of the naive method estimate. To illustrate this point, we compare the two methods for the “shift” detector model where  $\lambda_s/R = 0.1$  (Figure 9).

In an additional study, we simulate realizations of  $N$  that are uniformly distributed between 50 and 1200. The Cartesian coordinates of each event location are randomly generated so that the radial location of a random event is uniformly distributed between 0 and  $R$ . We compute the test statistic

$$z = \frac{n - Np}{\sqrt{Np(1-p)}} \quad (16)$$

for each event. Assuming that our binomial assumption is correct, the pdf of  $z$  should be well approximated by a unit normal (Gaussian) distribution centered on 0. That is, the expected value and variance of  $z$  should be approximately 0 and 1. Clearly, for events near the wall, the observed variability of  $z$  is inconsistent with the binomial assumption (Figure 10). We attribute this high variability to the incomplete coverage of the walls by the detectors. For instance, in some cases events can occur near the wall in gaps between detectors. For such cases, almost all of the emitted photons traveling radially outward could be lost to the walls. Assuming that the other half of the photons that travel radially inward are detected with probability  $p$ , the overall detection probability would be approximately  $p/2$  rather than  $p$ . We attribute the apparent outliers for CASE A in Figures 5,6, and 7 to a similar wall effect.

For the “no-shift” detection model, the probability of detecting a photon that is emitted at the center of the spherical detection volume is  $p_c = 0.75295(13)$ . Based on  $p_c$ , we predict the probability of detecting a photon emitted from the center of the spherical detection volume to be  $p = 0.65994(16)$  using the formula  $p = p_c(1 - 0.5(1 - p_c))$  presented in Section 4.2. For simulated events where the initial radial position of the photon was uniformly distributed between 0 and  $0.9 R$ , we compute the ratio of detected to emitted photons

for scattering lengths  $\lambda_s/R = 0.01, 0.1, 1, \infty$ . For the “no-shift” detection model, this ratio is respectively 0.7536(3), 0.7526(3), 0.7529(3), and 0.7528(3). For the “shift” detection model, this ratio is respectively 0.6607(3), 0.6605(3), 0.6606(3) and 0.6604(3).

## 5 Discussion

Since the variability of the Centroid method estimate of radial location is higher than the variability of the ML method estimate, we expect the ML method to be a more powerful method for background discrimination applications. The relative performance of the two methods should be most dramatic for low count situations. Quantifying this relative performance is a subject for further study.

For an actual energy spectrum of interest, due to wall effects, the actual distribution of events of interest that produce  $n$  observed events might deviate slightly from a uniform distribution even if the actual distribution of events that yield  $N$  has a uniform distribution. If this deviation from uniformity is significant, we should account for it when constructing critical levels of statistical tests to determine whether an event is due to a background event.

It is reasonable to assume that the number of emitted scintillation photons is a realization of a Poisson process with a rate parameter proportional to the energy deposited by the event. Imagine that some physical process of interest produces events with energy deposit spectrum  $f(E)$ . The spectrum  $f(E)$  is a pdf in energy space. Due to the Poisson assumption, the number spectrum  $g(N)$  generated by this process will be proportional to the convolution of  $f(E)$  with a transition matrix  $p(N|E)$ . The spectrum for observed counts  $q(n)$  is

$$q(n) \propto \sum_N \int_E \int_{\mathbf{x}_s} f(E)p(N|E)h(n|N, \mathbf{x}_s)d\mathbf{x}_s dE, \quad (17)$$

where  $h(n|N, \mathbf{x}_s)$  is a transition matrix that accounts for incomplete detector coverage and position effects like the wall effects noted in this work. Estimation of the true energy spectrum of interest  $f(E)$  from the empirical count distribution observed in an experiment is a challenging statistical inverse problem worthy of further study. However, it is possible to develop statistical tests to determine whether a theory explains the observed data without “solving” the inverse problem if, given a theoretical estimate of  $f(E)$ , we can predict the count spectrum for the observed data.

## 6 Summary

We estimated the radial location of an ionizing radiation event that produced multiple photons at a point within a spherical detection volume, based on the observed count data collected by detectors mounted at the spherical boundary of the detection volume. We neglected absorption but accounted for Rayleigh scattering as well as photon conversion and re-emission at the detectors. In one method, the predicted value was a polynomial function of the centroid of the observed count data. In the second method, the predicted value was a polynomial function of the approximate maximum likelihood estimate of the radial location. In both cases, the polynomial correction models were constructed from calibration data. In general, the ML method estimate was more accurate than the Centroid method estimate. In this work, our ML estimate of location was determined using a transition matrix that neglects scattering and detector conversion of photons. We corrected our estimate of radial location in a post-processing step using a calibration model. For the case of negligible absorption, as the scattering length decreased, the accuracy of the corrected estimate improved. For the case where absorption is significant, we may not observe this sort of improvement.

The event reconstruction methods presented in this work do not account for photon absorption in neon. For the case where absorption is significant, we would either modify our methods or adopt a different method. For the case where absorption is significant, a spatial ML method based using estimate of the true transition matrix, as suggested in [6], is a promising approach. However, as we mentioned earlier, even if one has a perfect estimate of the transition matrix accounting for scattering and other effects such as absorption, the ML method estimate of radial position may still be biased. Additional calibration experiments may be necessary to quantify detector efficiency even if we know the true transition matrix.

We estimated the intensity of the event using the ML method and a much simpler scheme. In the simpler scheme, the estimate is the number of detected photons divided by a detection probability factor. In general, the simpler method was as good as or better than the ML method. For the events near the wall, the variability of the ML estimate was higher than the variability of the simple method.

In future work, we will study how well our event reconstruction method discriminates events of interest from background events for simulated data. In particular, we plan to study the relative performance of the Centroid and Maximum Likelihood methods. We expect the relative performance of the two methods to be most dramatic for low count situations. For high count situations, both methods could be useful. For instance, the Centroid method

might serve to validate results obtained by the Maximum Likelihood method. In an actual experiment, multiple-point background events can occur because background gamma rays can deposit fractional amounts of their total energy. Additional simulation studies indicate that we can discriminate such multiple-point background events from single-point events of interest.

Our work demonstrates the feasibility of spatial methods for event reconstruction for the case where scattering is significant but absorption is negligible. We developed calibration models to adjust estimates of the radial location of an event based on simulated calibration data. In a simulation, one can sample calibration data throughout the entire detection volume. In a real experiment, one might not have such freedom. If sampled points are not sufficiently representative of all points in the detection volume, the accuracy of the calibration model could be affected. Thus, validation of empirical calibration methods for an actual experiment is an important topic for further study. Other important topics for further study include: energy spectrum estimation, quantification of detector efficiency and false detection rate as a function of the number of detected counts, and development of statistical hypothesis tests for neutrino models.

**Acknowledgements** We thank Adele Peskin of NIST for visualization work. We thank Andrew Hime of Los Alamos National Laboratory and Grace L. Yang of the University of Maryland and NIST for useful comments. The work of Daniel N. McKinsey was supported in part by the National Science Foundation under grant number PHY-0226142.

## References

- [1] D. N. McKinsey and J. M. Doyle, *J. Low. Temp. Physics*, 118, 361 (2000)
- [2] C. J. Horowitz, K. J. Coakley and D. N. McKinsey, to be published in *Phys. Rev. D*.
- [3] Super-Kamiokande collaboration, Y. Fukuda et al., *Phys. Rev. Lett.*, 82, 1810 (1999)
- [4] Super-Kamiokande collaboration, Y. Fukuda et al., *Phys. Rev. Lett.*, 82, 2430 (1999)
- [5] J. F. Beacom, W. M. Farr, and P. Vogel, *Phys. Rev. D* 66, 033001 (2002)
- [6] S. Moriyama (XMASS Collaboration), 4th International Workshop on the Identification of Dark Matter, York, England, 2-6 September 2002. <http://www.shef.ac.uk/~phys/idm2002/talks/pdfs/moriyama.pdf>
- [7] F. Gao, H. Niu, H. Zhao and H. Zhang, *Image Vision Computing*, 16, 703 (1998)
- [8] L. A. Shepp and Y. Vardi, *IEEE Trans. on Med. Imag.* 1 113 (1982)
- [9] Y. Vardi, L. A. Shepp and L. Kaufman, *J. of the Amer. Stat. Assoc.*, 80 389 8 (1985)
- [10] A. Krol, J. E. Bowsher, S. H. Manglos, D. H. Feiglin, M. P. Tornai and E. D. Thomas, *IEEE Trans. on Med. Imag.* 20 3 218 (2001)
- [11] P. P. Bruyant, *Journal of Nuclear Medicine*, 43 10 1343 (2002)
- [12] Y. Bard, *Nonlinear Estimation*, Academic, New York (1974)
- [13] G. L. Yang and K. J. Coakley, *Phys. Rev. C*, 63 014602 (2002)
- [14] W. R. Nelson, H. Hirayama and D. W. O. Rogers, *The EGS4 Code System*, SLAC-R-265, Stanford University, (1985)
- [15] D. E. Peplow, *Nucl. Sci. and Engin.*, 131, 132, (1999)
- [16] R. H. Hardin, N. J. A. Sloane and W. D. Smith, *Tables of Spherical Codes with Icosahedral Symmetry*, [www.research.att.com/njas/icosahedral.codes/index.html](http://www.research.att.com/njas/icosahedral.codes/index.html). Maintained by N. J. A. Sloane, AT&T Shannon Lab, 180 Park Ave, Room C233, Florham Park, NJ
- [17] E. L. Lehmann, *Theory of Point Estimation*, John Wiley and Sons, New York (1983)
- [18] D. M. Gay, Computing Optimal Locally Constrained Steps, *Siam J. Sci. Statist. Comput.* 2, 186 Philadelphia (1981)
- [19] D. Kahaner, C. Moler and S. Nash, *Numerical Methods and Software*, Prentice Hall, New York (1988)



- [20] W. Feller, *An Introduction to Probability Theory and Its Applications*, Vol. 2, John Wiley and Sons, New York (1966)
- [21] A. M. Wood, F. A. Graybil and D. C. Boes, *An Introduction to the Theory of Statistics*, McGraw Hill, New York (1974)
- [22] B. Efron and R.J. Tibshirani, *An Introduction to the Bootstrap*, Monographs on Statistics and Applied Probability 57, Chapman and Hall, New York (1993)

Table 1. Calibration model parameters for Maximum Likelihood Estimate. RMSE is the square root of the mean square prediction error, adjusted for degrees of freedom, computed from all calibration data. The number of counts in each calibration data set varies from 50 to 1200.

$\lambda_s/R$	$\widehat{\alpha}_1$	$\widehat{\alpha}_2$	$\widehat{\alpha}_3$	RMSE
no-shift				
$\infty$	0.894(16)	0.261(46)	-0.156(33)	0.0357
1	0.779(15)	0.312(41)	-0.072(28)	0.0308
0.1	0.602(14)	0.264(39)	0.182(26)	0.0271
0.01	0.618(9)	0.047(25)	0.368(17)	0.0246
shift				
$\infty$	1.316(20)	0.023(55)	-0.366(37)	0.0501
1	1.096(14)	0.347(40)	-0.455(28)	0.0435
0.1	0.856(11)	0.419(37)	-0.258(28)	0.0344
0.01	0.855(12)	0.189(38)	-0.033(28)	0.0328

Table 2. Calibration model parameters for Centroid Estimate. RMSE is the square root of the mean square prediction error, adjusted for degrees of freedom, computed from all calibration data. The number of counts in each training data set varies from 50 to 1200.

$\lambda_s/R$	$\widehat{\beta}_1$	$\widehat{\beta}_2$	RMSE
no-shift			
$\infty$	1.483(10)	0.0108(194)	0.0465
1	1.326(6)	-0.0525(115)	0.0370
0.1	1.049(5)	0.0167(64)	0.0291
0.01	0.991(4)	0.0176(53)	0.0257
shift			
$\infty$	2.094(21)	-0.113(56)	0.0675
1	1.826(15)	-0.084(35)	0.0563
0.1	1.475(8)	0.006(14)	0.0438
0.01	1.386(7)	0.018(14)	0.0415

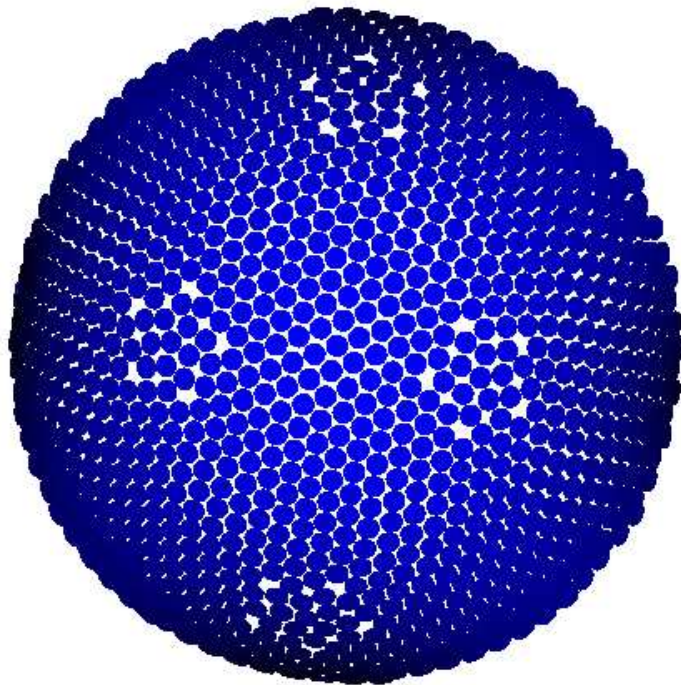


Figure 1. Detector geometry for simulation study.

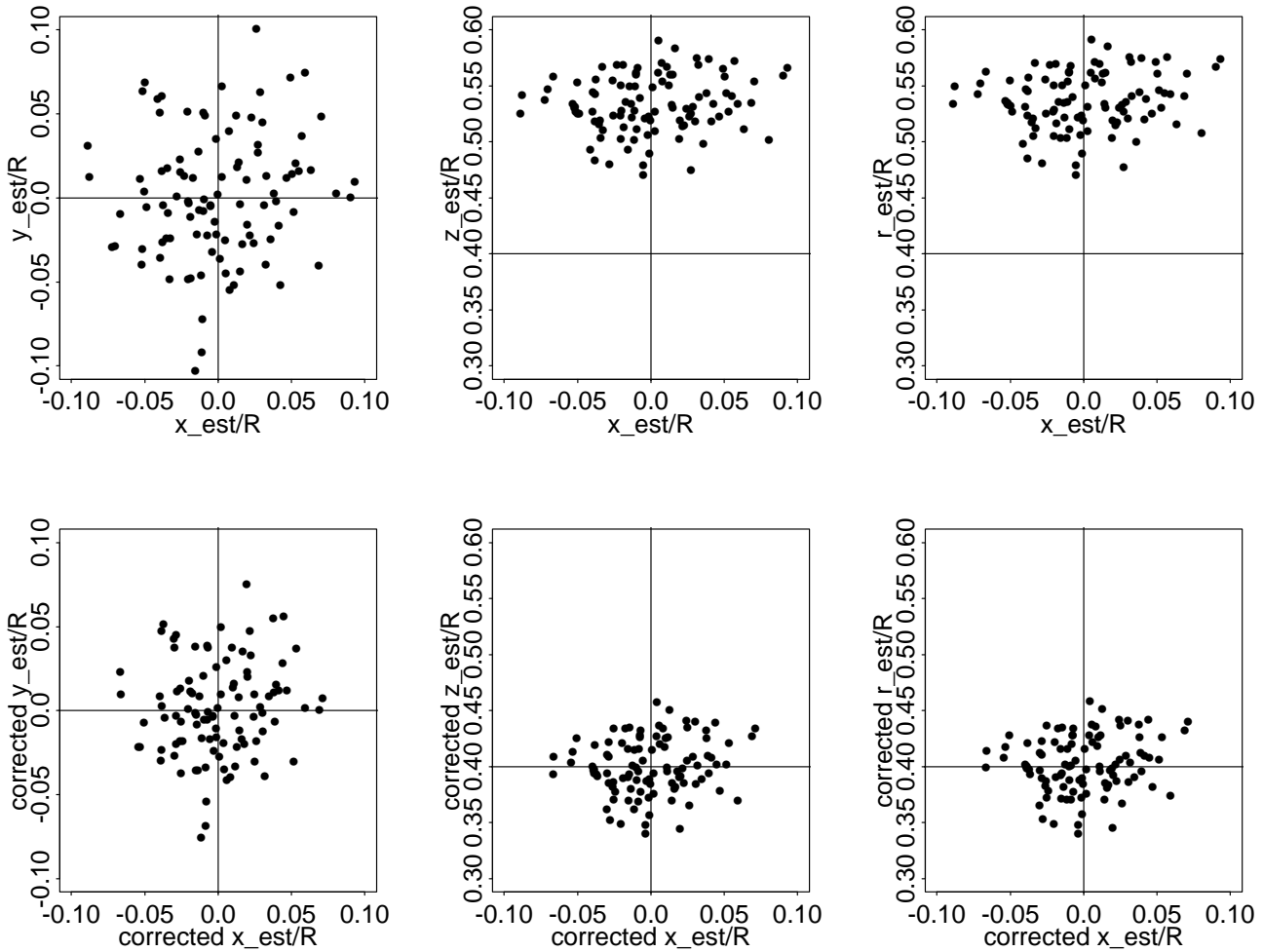


Figure 2. Top row: 100 realizations of the uncorrected  $x,y,z$  and radial components of the Maximum Likelihood estimate of position. Bottom row: Corrected version of top. True position is  $(x,y,z) = (0,0,0.4R)$ . The scattering length is  $\lambda_s = 0.1 R$ . “No-shift” detection model. The modified intensity parameter is  $\lambda_{p_e} = 400$ .

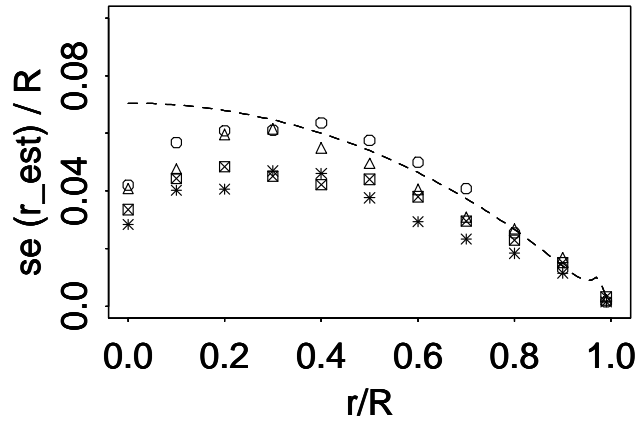
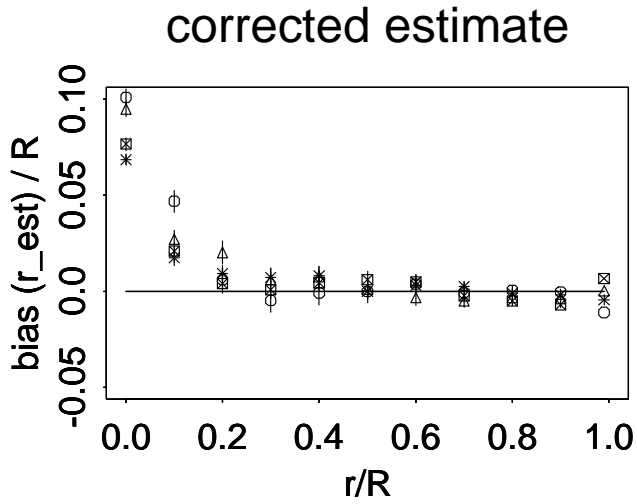
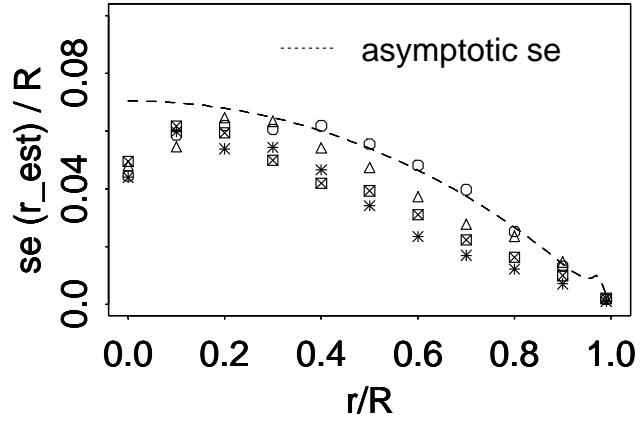
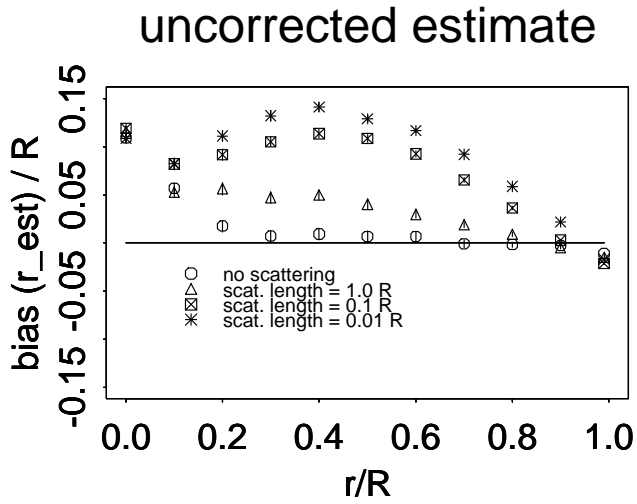


Figure 3. Bias and standard error of corrected and uncorrected radial estimates of position for data simulated on a grid along the  $z$ -axis. The modified intensity  $\lambda p_e$  is 200. “No-shift” detection model.

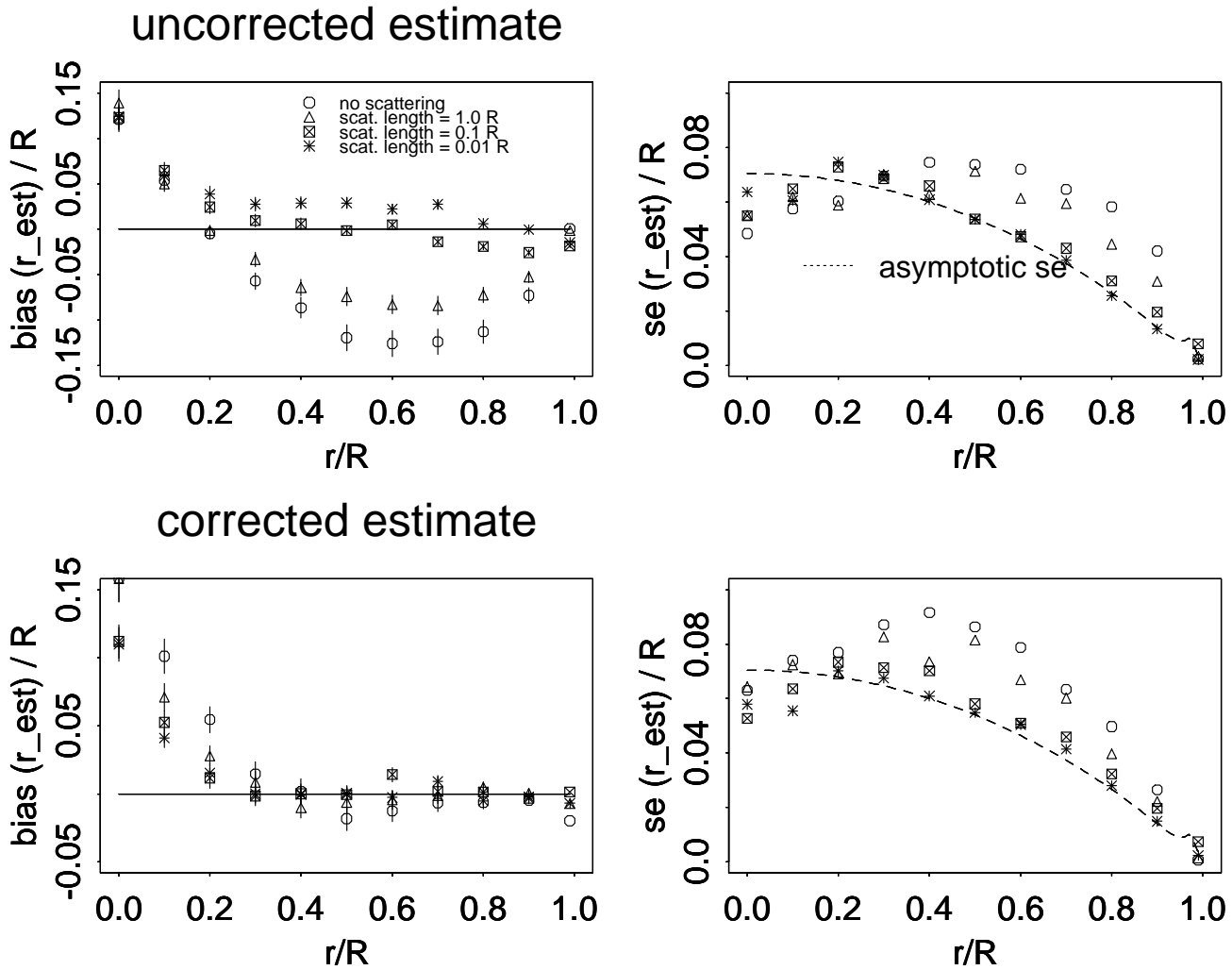


Figure 4. Bias and standard error of corrected and uncorrected radial estimates of position for data simulated on a grid along the  $z$ -axis. The modified intensity  $\lambda p_e$  is 200. “Shift” detection model.

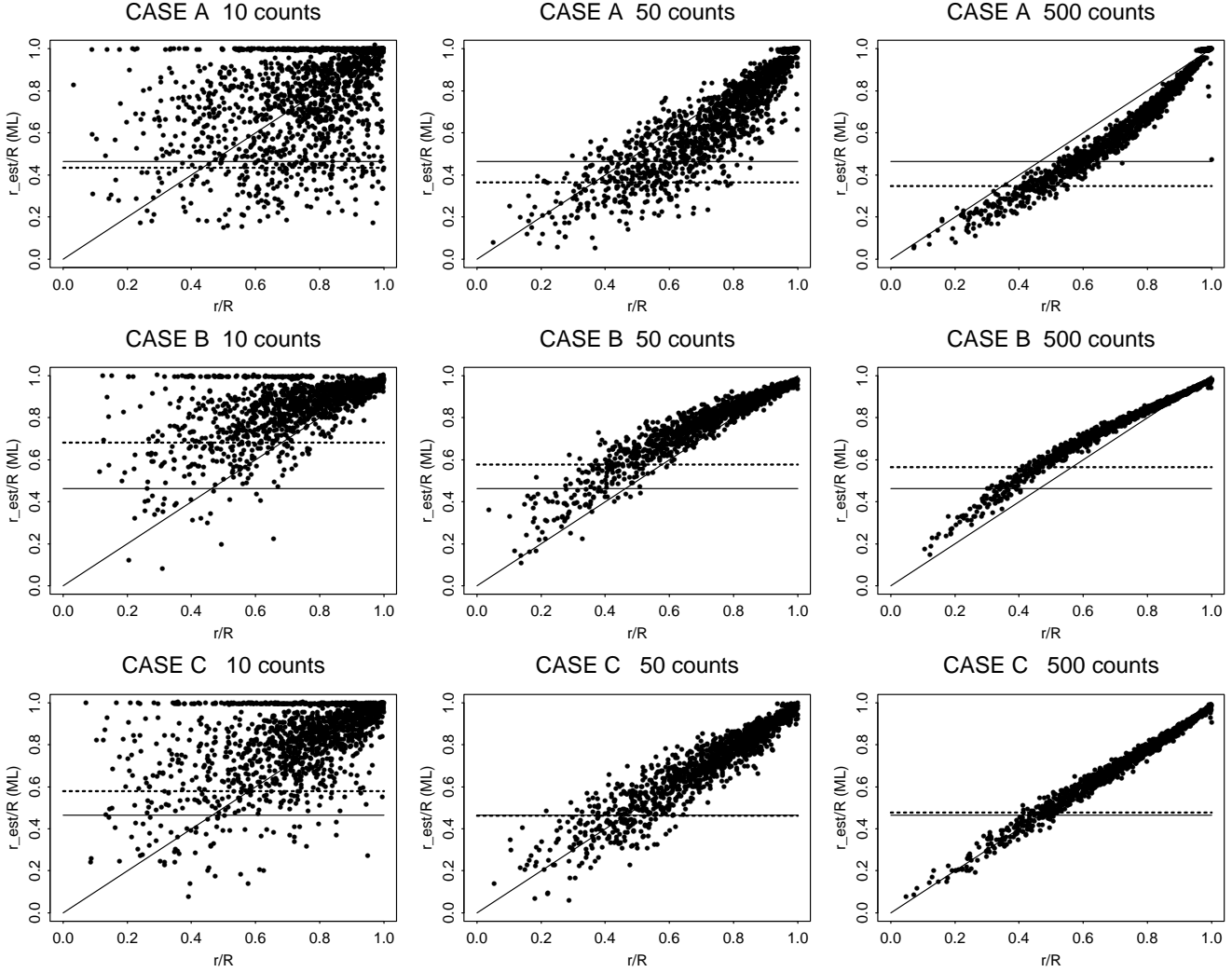


Figure 5. Uncorrected Maximum Likelihood model estimates of radial position for events that occur uniformly within the sphere. CASE A:  $\lambda_S = \infty$  and “shift” detection model CASE B:  $\lambda_S = 0.1R$  and “no-shift” detection model. CASE C:  $\lambda_S = 0.1R$  and “shift” detection model. For each plot, we show the 0.1 quantile of the prediction (dashed line) and the  $r_p$  level.



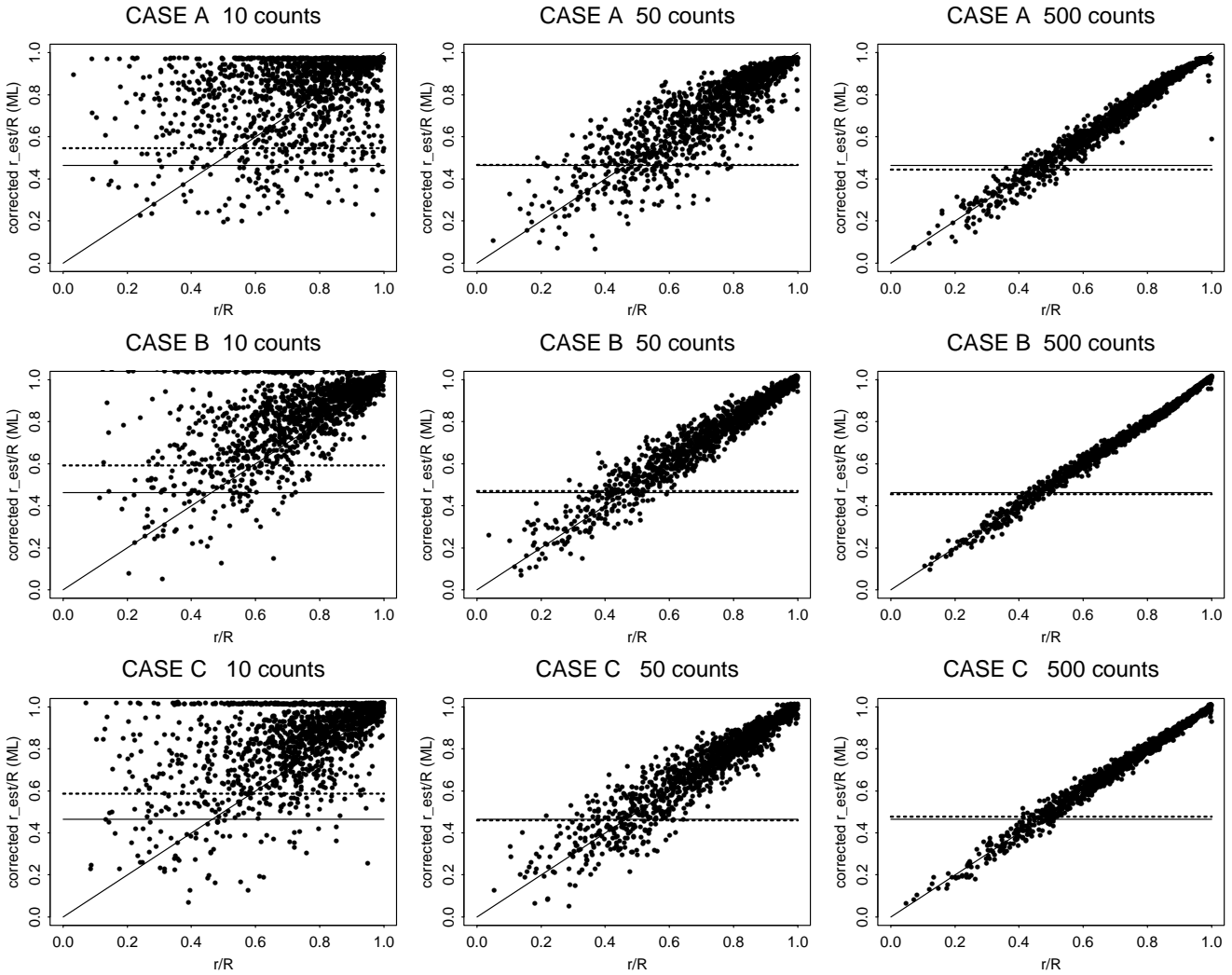
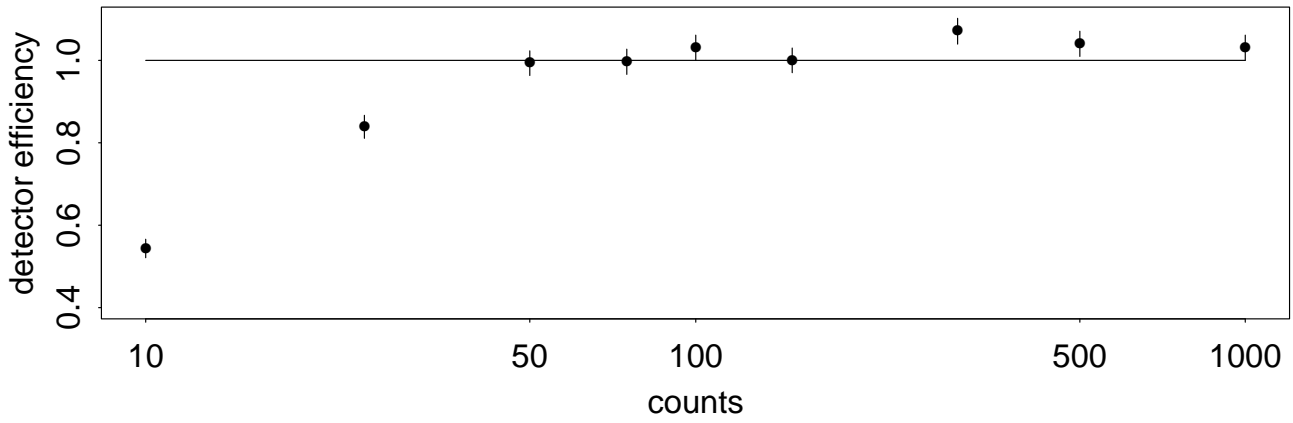


Figure 6. Corrected Maximum Likelihood model estimates of radial position for events that occur uniformly within the sphere. Same data as in Figure 5.

### 10 percent fiducial volume



### 1 percent fiducial volume

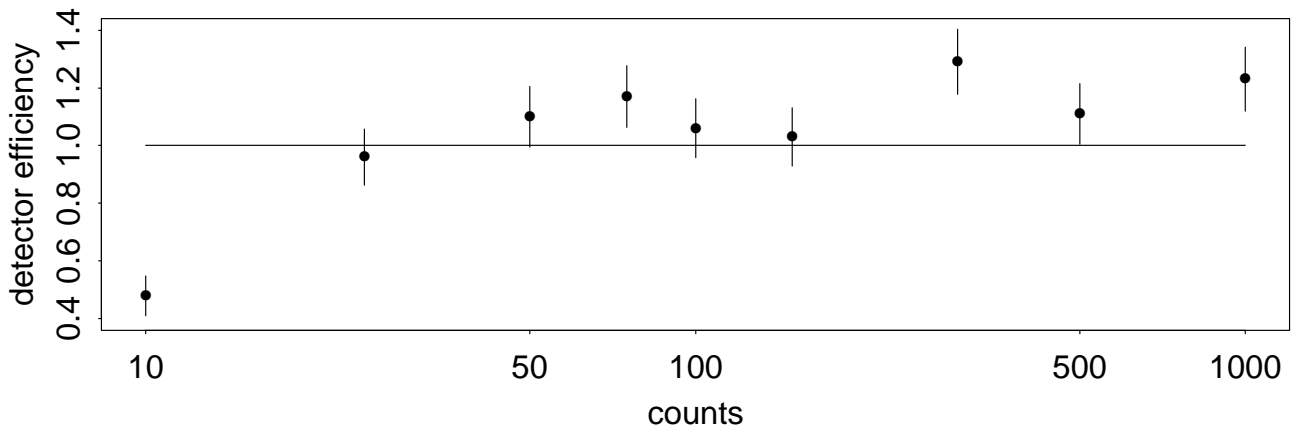


Figure 7. Detector efficiency for 1 % and 10 % fiducial volumes for  $\lambda_s/R = 2/9$  ( $\pm 1$ -sigma uncertainty intervals shown). “Shift” detection model.

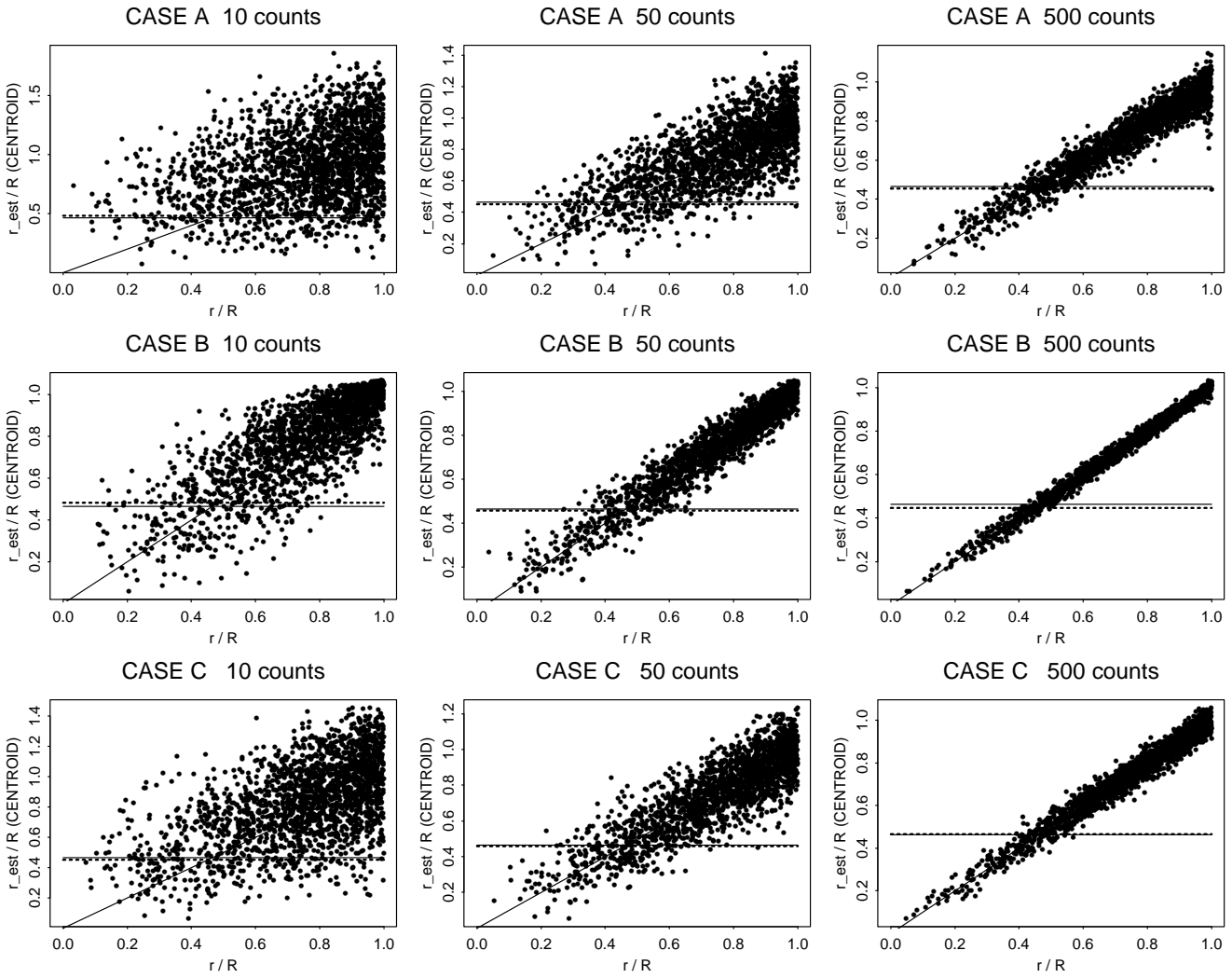


Figure 8. Predicted radial estimate based on centroid. Same data as in Figure 5.

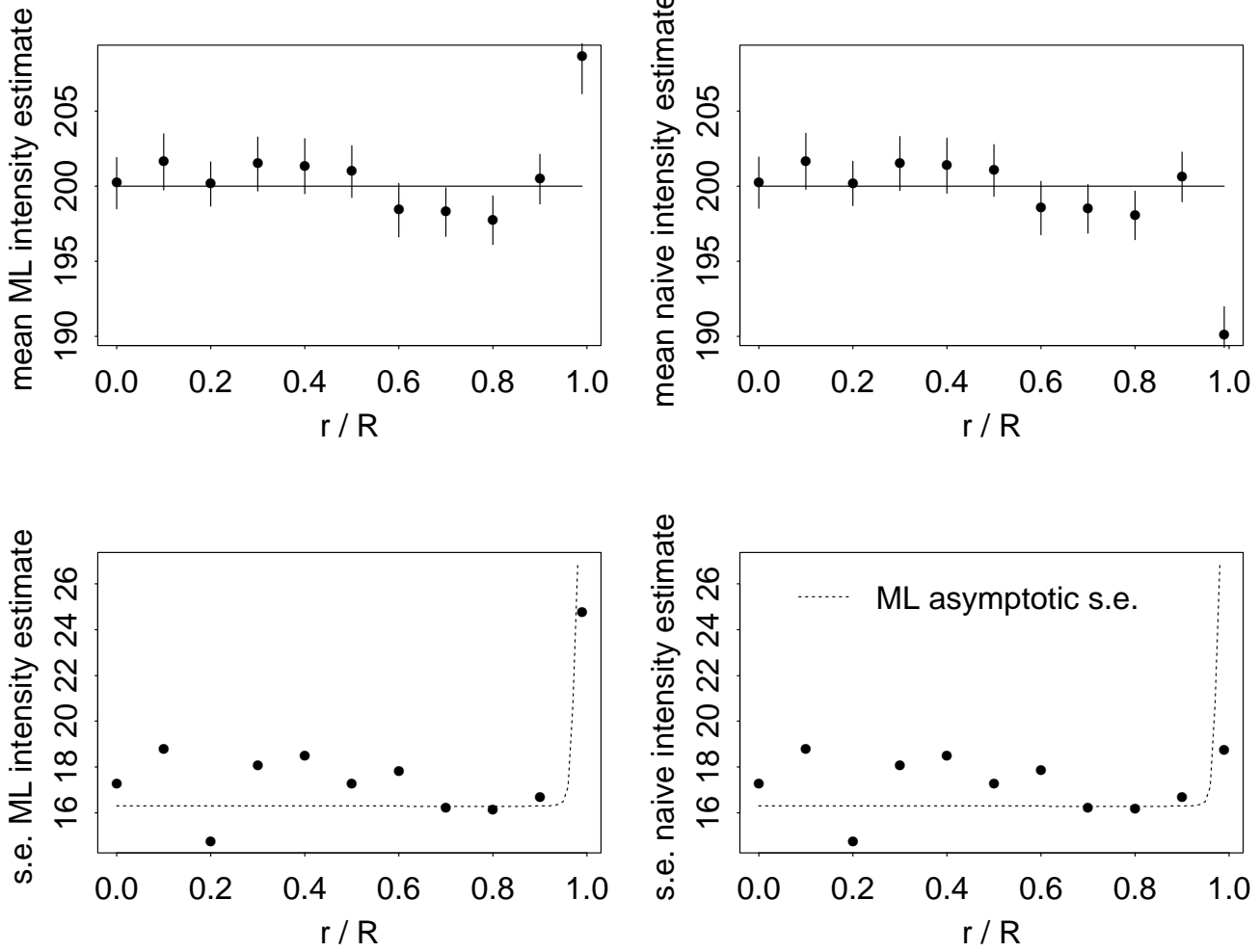


Figure 9. For the “shift” detection model and  $\lambda_s/R = 0.1$ , we compare the mean and standard error of two estimates of modified intensity for the case where event locations are on the  $z$  axis. The modified intensity is  $\lambda p_e = 200$ .

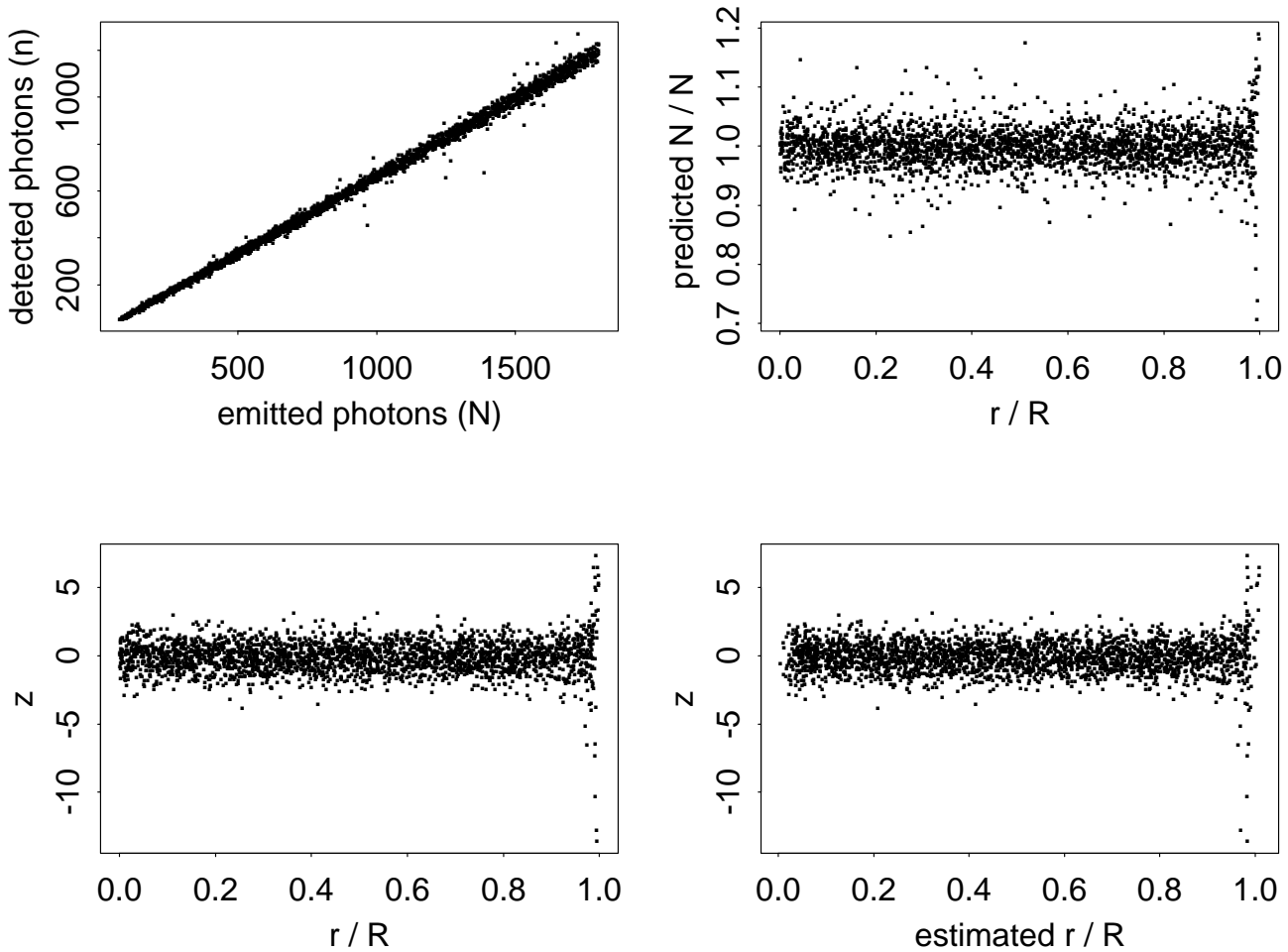


Figure 10. “Shift” detection model and  $\lambda_s/R = 0.1$ . We predict  $N$  based on the number of detected photons  $n$  using our “naive” estimation model. If our “naive” model for predicting modified intensity is valid,  $z$  should be approximately a Gaussian random variable with expected value and standard deviation equal to 0 and 1.